A time-of-flight mass filter for ion and cluster ion photodissociation studies

J. A. Syage and J. Steadman

Aerophysics Laboratory, The Aerospace Corporation, P. O. Box 92957, Los Angeles, California 90009

(Received 9 November 1989; accepted for publication 13 November 1989)

A sensitive method is described for detecting photodissociation products from a specific ion or cluster ion in the absence of the initially formed fragment ions that would otherwise interfere with the signals of interest. By using a simple pulse sequence, the conventional three-grid time-of-flight (TOF) assembly can be operated as a low-mass rejection filter capable of eliminating all ions below an adjustable threshold mass value. The method has been applied using different ionization sources [e.g., picosecond and nanosecond photoionization, and electron impact (EI) ionization]. Molecular-beam applications are demonstrated for (1) high-resolution resonance ion dissociation spectroscopy of rovibrationally cold ions, and (2) stepwise solvation of neat and seeded cluster ions formed by either photoionization or EI ionization. The low-mass filter (LMF) is especially powerful for cluster ion photodissociation studies. For example, the elimination of successively larger cluster ions leads to photofragment mass spectra that can uniquely establish the photodissociation and metastable decay fragments from specific cluster ions.

INTRODUCTION

The study of ion photodissociation is often faced with the difficulty of distinguishing primary events (e.g., dissociative ionization) from the secondary events of interest (e.g., photodissociation).[1,2] As an example, we cite the common problem of detecting a weak photofragment ion against a background of fragment ions formed in the initial ionization step. The problem is further compounded in photodissociation studies of cluster ions.[3] Not only are primary and secondary fragment ions difficult to distinguish, but the greater task of assigning the secondary fragment ions of interest to specific cluster ion parents adds to the experimental complexity.

The available methods for selecting specific ion masses for ion photodissociation studies depend primarily on tandem mass spectrometer designs. A variety of dispersive mass filter/analyzer designs (e.g., Wein filter) are used in such broad-based experimental techniques as ion beam[4] and ion cyclotron resonance[5,6] (ICR) spectroscopy. In Fourier transform ICR,[6] a pulsed rf field can be used to expel all but one mass from the ion trap. Molecular-beam adaptations for studying mass-selective ion photodissociation include in-line quadrupole[7,8] or time-of-flight[9,10] devices that precede a final detection mass spectrometer.

We demonstrate a new concept for mass-selected ion photodissociation studies that requires a single time-of-flight mass spectrometer (TOFMS) and is therefore adaptable to conventional molecular-beam mass spectrometer systems. By applying a simple pulse sequence, the standard three-grid TOF ion optics assembly can be operated as a low-mass rejection filter that eliminates all primary ions (i.e., those formed by the initial ionization event) below an adjustable cutoff value. This makes possible the detection of secondary photofragment ions against a zero background. More importantly, it allows one to tune the range of masses that one wishes to retain for photodissociation studies. We will demonstrate two important applications: (1) the recording of resonance ion dissociation spectra, and (2) the recording of cluster ion dissociation mass spectra from *specific* parent cluster ions. The first capability can be achieved by other relatively straightforward molecular-beam methods, though arguably not with as much ease or sensitivity as the present approach. The second capability is perhaps more novel in that mass specific cluster ion studies have always been the domain of elaborate double-mass spectrometer molecular-beam configurations.

Finally, it is important to contrast the present method to the capabilities of a reflectron TOFMS. The reflectron is an energy filter that can detect a change in ion kinetic energy that occurs by dissociation to a lower mass ($\Delta E = \Delta m v^2/2$).[11,12] This allows fragment ion mass spectra to be recorded in the absence of parent ions. It is also possible to determine the fragment parentage by determining Δm from a measure of ΔE.[11] However, the reflectron can only detect dissociation that occurs on a timescale comparable to the initial acceleration period (>100 ns). Although, the device has proved very important to the study of metastable ion decay, it has yet to be operated in a mode that enables the detection of more rapid dissociation. The present TOF adaptation uses mass rather than energy filtering; the photodissociation pulse occurs *after* the low-mass rejection period so that fragments are detected, independent of dissociation rate, against a zero background. Naturally, the present method is applicable to reflectrons, as it is for all TOF devices.

I. EXPERIMENT

The focus of this article is on the low-mass TOF filter device. The full details of the molecular-beam and data acquisition system are described elsewhere.[13] Briefly, the vacuum system consists of separate differentially pumped source and ionization chambers. The apparatus makes use of a home-built pulsed supersonic nozzle that is driven by a magnetic solenoid mechanism and is temperature controlled. Typical pulsed expansion conditions in the source chamber are 25-psi Ar or He, 500-μm nozzle diam, 400-μs pulse width, 2-cm nozzle-skimmer distance, and 1-mm diam skimmer. A TOF mass spectrometer resides in the ionization

 0034-6748/90/041204-07$02.00

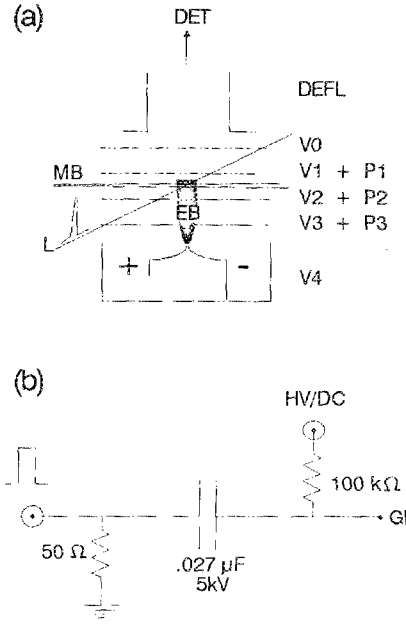

FIG. 1. (a) Configuration of the crossed electron-laser-molecular beam ion optics assembly. The direct current (dc) grid voltages are designated by V and the pulsed voltages by P. Deflector plates (DEFL) are used to compensate for ion drift resulting from the molecular beam (MB) velocity. Laser pulses are denoted by L and the detector by DET. (b) Circuit for applying a high voltage (HV) dc bias to a voltage pulse. Unshielded cable was used after the 50-Ω termination to avoid ringing.

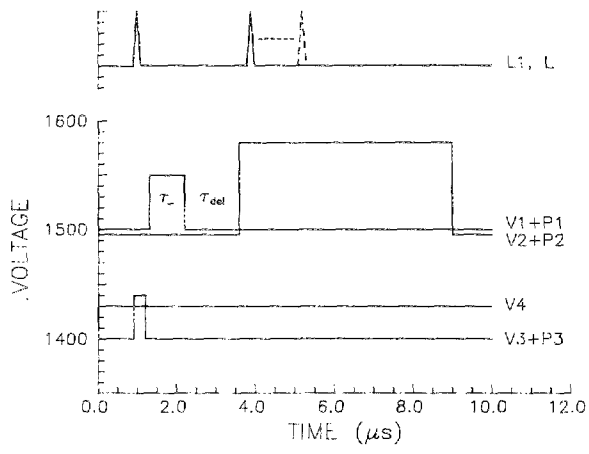

FIG. 2. Pulse sequence and typical voltage levels used for low-mass filter (LMF) applications. The potential difference between grids 1 and 2 defines the field gradient across the excitation region. Multiphoton ionization (L1) or electron impact ionization (gated on by pulse P3) occurs in a field-free environment (i.e., V1 = V2). Low-mass ions are ejected from the ionization region by P1 (of duration τ_-) in a direction away from the detector. The remaining high masses are then reversed by P2 and cross with the photodissociation pulse L, before being accelerated toward the detector. The delay period τ_{del} is typically zero except for studies of metastable decay.

chamber. The ambient base pressure in the ionization chamber is typically 3×10^{-8} Torr, rising to about 2×10^{-7} Torr during operation of the pulsed nozzle at 10 Hz.

The TOF ion optics consist of the conventional three-grid Wiley and McLaren[14] configuration represented by V0, V1, and V2 in Fig. 1. The additional elements V3 and V4 are part of a pulsed electron impact (EI) ionization source that is independent of the low-mass filter (LMF). The EI source, described in detail elsewhere,[15,16] is represented in the overall LMF pulse sequence in Fig. 2, and described briefly. Electrons are generated from a hot tungsten filament. An electron-beam pulse is admitted to the field-free excitation region by applying to V3 a 40-V gate pulse P3 (duration 200–400 ns). The electron beam is collimated to a diameter of approximately 5 mm by the apertures at V2 and V3 to ensure good overlap with the molecular beam. Electron energies relative to V2 are varied by adjusting the voltage applied to V3 and V4, which differ by a fixed potential drop of 30 V. The excitation region is maintained field free during the electron-beam pulse by applying a constant (1500 V) potential to grids V1 and V2. The EI source was designed for narrow electron energy distributions (by using a hairpin filament) rather than for large fluxes. Consequently, the ionization efficiency is only about 10^{-6}.

The pulse sequence for low-mass rejection and high-mass detection is illustrated in Fig. 2 for EI or laser (L1) ionization. Following ionization, a voltage pulse P1 is applied to V1 to create a negative field gradient that accelerates ions in a direction away from the detector. The lighter masses, which accelerate faster, are the first to exit the extraction region through grid V2. After an appropriate time, the P1 pulse is dropped and the P2 pulse is applied to V2, thereby creating the positive field gradient that accelerates the remaining higher masses toward the detector. A TOF mass spectrum is, thus, obtained that is free of all signals below a selected mass. The production of low masses by photodissociation (laser pulse L) or metastable decay *after* the P1 rejection pulse, would then appear on this zero background. The P1 pulse amplitude and duration (typically 20–80 V, 1–3 μs) defines the cutoff mass value, and is discussed in Sec. II. The P2 extraction voltage is chosen to optimize space focusing, and the duration is maximized to extract the highest masses of interest. [At present, our P2 pulse generator is limited to about 4 μs at 50–75 V, and hence the TOF mass resolution for larger cluster ions (e.g., $m > 300$ amu) deteriorates quickly]. An alternative LMF arrangement, which dispenses with the need for a P1 pulse, can be achieved by applying a continuous negative voltage across the ionization region (by reducing V2 or increasing V3) and then applying a P2 pulse to overcome the negative bias so as to direct the remaining higher masses toward the detector. This method has the advantage of requiring a single pulse generator; however, it does not allow field-free ionization, should this be important (e.g., for constant energy EI ionization). When using EI ionization prior to nanosecond laser photodissociation, it was necessary to externally trigger the laser Q-switch in order to synchronize the laser pulse with the P1, P2, and P3 pulse generators.

II. PRINCIPLE OF OPERATION

The low-mass rejection filter operates by first applying a potential gradient (field) across the ionization region that is negative with respect to the direction of the detector. This accelerates the ions away from the detector with the lighter masses exiting the lower V2 grid before the heavier masses. By reversing the field, the remaining higher masses are accelerated toward the detector to give a TOF mass spectrum that

has the primary low masses filtered out. The amplitude and duration of the rejection pulse defines the cutoff mass value. These considerations can be described by simple equations[14] if we assume parallel plate flat fields. We relate the position s(cm) and velocity v(cm/μs) of an ion as a function of the field E(V/cm), time t(μs), mass m(amu), and the charge $q(\pm 1)$ as follows:

$$s(t+t_i) = s(t_i) + v(t_i)t + 0.482qEt^2/m \quad (1)$$

$$v(t+t_i) = v(t_i) + 0.965qEt/m \quad (2)$$

where t_i is the initial time for t. The proportionality constants are specific to the units chosen above. The low-mass filter (LMF) benefits from the dependence $s \propto 1/m$ that occurs in an acceleration field as compared to $s \propto 1/m^{1/2}$ that occurs in a field-free region. The behavior arises because lighter masses, compared to heavier masses, not only travel at higher velocities at a given energy, but also increase in velocity more rapidly in an acceleration field.

We have calculated ion trajectories based on the LMF pulse sequence in Fig. 2. The value of E as a function of time depends on the pulses P1 and P2 and the grid region in which the ions reside. The selectivity of the LMF near the threshold mass m_0 is represented in Fig. 3. In Fig. 3(a), the results for masses similar to m_0 that originate from the same initial position indicate that the cutoff condition can be very sharp for relatively small ionization volumes. Examples of ion trajectories for the same mass, but different initial positions, are plotted in Fig. 3(b) and show that the LMF resolution broadens for larger ionization volumes.

We choose to analyze the LMF resolution by deriving a function that describes the fraction of ions that are detected at each mass for some given ion density distribution. The conditions for rejecting mass m depend on the initial ion position and can be determined by solving for the conditions under which $v(t+t_i) = 0$ at $s(t+t_i) = 0$ (i.e., when the ion trajectory turnaround occurs at precisely the lower grid position). By adopting the LMF pulse sequence in Fig. 2, one then obtains from Eqs. (1) and (2) (cf. Appendix) the relation

$$mx_m(0) = 0.482\frac{E_-(E_- - E_+)}{E_+}\tau_-^2, \quad (3)$$

where E_- is the negative field across the ionization region during the P1 rejection pulse period τ_-, and E_+ is the positive field that follows as a result of the P2 extraction pulse period. We have expressed s as a fraction x of the V1-V2 grid spacing l (i.e., $x = s/l$), such that $x = 0$ and $x = 1$ correspond to the lower V2 and upper V1 grid positions, respectively. Equation (3) assumes successive P1 and P2 square pulses with no delay, and a P2 pulse duration τ_+ that is longer than the time required for ions and of mass m to turn around. The term $x_m(0)$ denotes the initial ($t = 0$) position for which ions of mass m turn around at precisely the lower grid position. Hence, ions of the same mass at positions $x > x_m$ will be detected and those at $x < x_m$ will be rejected. The overall fraction of ions that are detected at a given mass is calculated by integrating over the ion density distribution $n(x)$ for these two regions. We have assumed a $n(x) = \{1 - [(x - x_0)/\Delta x]^2\}^{-1}$ distribution which derives from the $\cos^2\theta$ distribution of a free-jet expansion.[17] For a distribution centered at x_0, the transmission function $T(m)$ for detection (cf. Appendix) is given by

$$T(m) = \frac{\tan^{-1}\chi(1) - \tan^{-1}\chi(x_m)}{\tan^{-1}\chi(1) - \tan^{-1}\chi(0)}, \quad (4a)$$

$$\chi(x) = \frac{x - x_0}{\Delta x}, \quad (4b)$$

$$x_m = m_0 x_0/m. \quad (4c)$$

Δx is the full width at half maximum (FWHM) of the ion density distribution expressed as a fraction of the grid spacing. The actual ion density distribution will depend on the molecular-beam conditions and the method of ionization. However, the transmission function is much more sensitive to the width of the distribution than to the shape of the distribution. We have therefore chosen a distribution function $n(x)$ that is realistic and integrable. We define the nominal threshold mass m_0 to represent the center position of the ion distribution. The values of m_0 and m are related to actual experimental conditions by Eq. (3).

Calculated transmission curves are presented in Fig. 4 as a function of the width Δx and position x_0 of the ionization volume. Clearly, the sharpness of the LMF depends on Δx; however, it is important to note that the onset to the detection of the lowest mass with respect to the nominal threshold m_0 also depends strongly on where the center of the ion distribution x_0 is positioned between the two grids. This can be understood by examining Eqs. (3) and (4c). To reverse the direction of an ion mass $m < m_0$ requires an initial position $x_m > x_0$. Because the V1 grid position defines the upper limit at $x = 1.0$, it follows that the lowest mass that can be reversed at this position is given by the simple relation m_0x_0. Consequently, *all ions of mass $m < m_0x_0$ are completely rejected, regardless of the size of the ionization volume.* From these considerations and Fig. 4, one concludes that greater filter resolution results by ionizing near the upper grid. The experimentally determined LMF resolution will be dis-

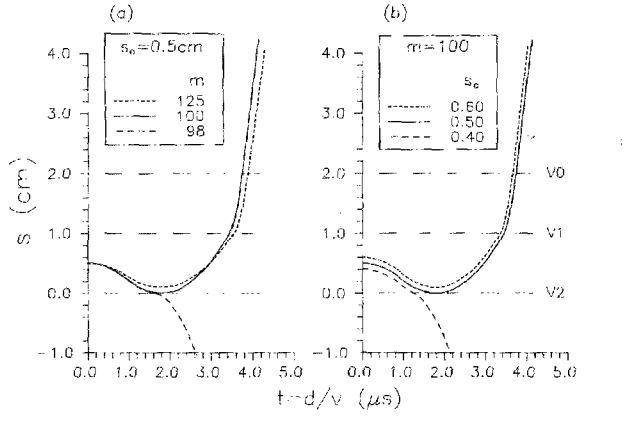

FIG. 3. Calculated ion trajectories s as a function of (a) mass m, and (b) initial position x_0. Actual grid positions are represented by the horizontal dashed lines. The position d of the ion along the molecular-beam direction is a function of the molecular-beam velocity v(5.6×10^4 cm/s for Ar). Calculations were based on; V1 = V2 = 1500 V, V3 = 1400 V, V0 = gnd, P1 = 60 V, P2 = 75 V, and $\tau_- = 1.0\,\mu$s.

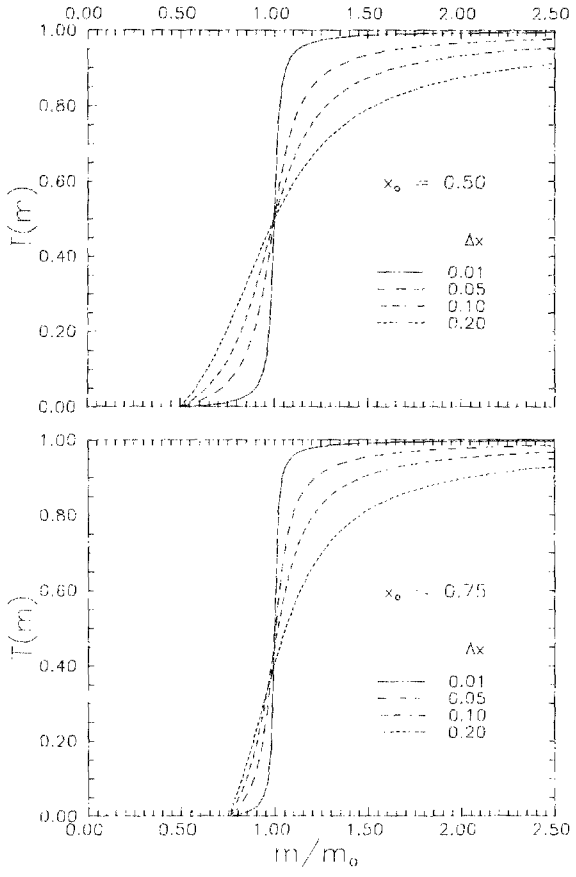

FIG. 4. Calculated transmission function for the retention of higher masses as a function of the position x_0 and width Δx of the ion distribution. Calculations were based on the parameters in Fig. 3 caption.

cussed shortly for cases involving spatially localized (MPI) and delocalized (EI) ionization.

III. APPLICATIONS

A common difficulty in ion photodissociation experiments is distinguishing between fragments formed during ionization and fragments formed by ion photodissociation. The LMF obviates this problem by effectively removing the lighter primary ion masses that might otherwise interfere with a desired photofragment ion. We demonstrate the LMF method for sensitive detection of ion photofragments for purposes of high-resolution ion spectroscopy and the study of photodissociation from size-specific cluster ions.

A. Ion photodissociation spectroscopy

There are very few examples of high-resolution vibronic spectra of polyatomic ions owing to the difficulty in producing rovibrationally cold ions and the tendency for larger ions to be nonfluorescing. One method for overcoming the latter difficulty is to detect a photodissociation resulting from the resonant absorption of light. The most striking example of high-resolution resonance ion photodissociation (RID) spectroscopy of a cold polyatomic ion is perhaps that for the $\tilde{A}$ state of CH_3I^+. High-resolution spectra have been recorded by producing cold ions by resonance-enhanced multiphoton ionization (REMPI)[18,19] and by electron impact (EI)[20] in a cold molecular beam. In these previous studies, it was necessary to delay the ionization and dissociation pulses so as to separate in time the CH_3^+ produced in both steps. In the REMPI work, Woodward *et al.*[18] relied on the different arrival times at the detector in monitoring the photodissociated CH_3^+. Schlag, *et al.*[19] refined the selectivity by applying a voltage pulse between the two laser pulses and using a reflecting electric field filter set to eliminate the higher energy CH_3^+ fragments formed by the first laser. The EI produced CH_3I^+ spectra[20] were recorded in our laboratory using the delayed photodissociation method of Woodward *et al.* Here we present spectra recorded under otherwise equivalent conditions except for the use of the low-mass rejection filter for discriminating photodissociated CH_3^+ from that initially produced by the ionization of CH_3I^+.

The effectiveness of removing the primary CH_3^+ signals and other undesirable signals from the desired photodissociation signal is shown in Fig. 5 for CH_3I^+ (5% in Ar). Primary ion signals below a prescribed mass are rejected before the photodissociation pulse [Fig. 5(b)]. The rejection efficiency of the strong Ar^+ signal, for example, is about 0.995. The introduction of a resonant photodissociation laser pulse produces a CH_3^+ photofragment signal that is now detected with high sensitivity against a zero background [Fig. 5(c)]. If some leakage of primary signal does occur at low mass, then the desired signal can be further isolated by delaying the photodissociation step (Fig. 2). A portion of the RID spectrum of the $\tilde{A} \leftarrow \tilde{X}(^2\Pi_{1/2})$ transition of CH_3I^+, acquired by detecting the CH_3^+ fragment ion, is presented in Fig. 5(d).

Finally, we estimate the sensitivity of detecting ion photodissociation using the LMF mode of detection. A molecular beam density of 10^{13} cm^{-3} for a 5% mixture of CH_3I in Ar, and an EI ionization efficiency of 10^{-6} produces a

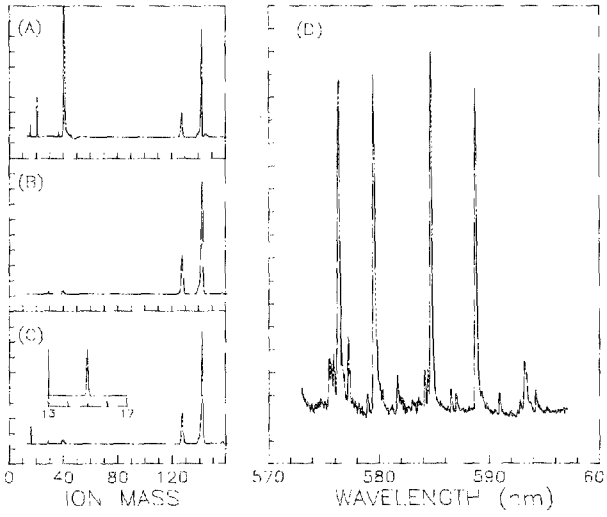

FIG. 5. (a) Conventional EI/TOF mass spectrum (Ar^+ peak has been clipped and is ~5× larger than shown). (b) Same, but with LMF pulse sequence (P1 = 65 V, τ = 1.0 μs); (c) Same as (b), but with photodissociation laser pulse (576.37 nm, 1×10^7 W/cm^2). (d) Portion of the one-photon RID spectrum of the $\tilde{A} \leftarrow \tilde{X}(^2\Pi_{1/2})$ transition of CH_3I^+ using the LMF mode of photofragment detection. Conditions for all spectra were 60-eV EI ionization, P2 = 75 V, and 5% CH_3I in 25 psi Ar.

CH_3I^+ concentration of 5×10^5 cm^{-3}. (This value ignores dilution due to formation of clusters, dissociative ionization, and excitation to other electronic states of CH_3I^+ that do not participate in the $\tilde{A}\leftarrow\tilde{X}(^2\Pi_{1/2})$ transition of interest.) Resonant dissociation of CH_3I^+ resulted in a signal-to-noise ratio of greater than 100 (with 100-pulse averaging) for detection of fragment CH_3^+. This corresponds to a photodissociation detection sensitivity on the order of 10^3 cm^{-3}. This excellent detection limit is due in part to the large ionization volume defined by the intersection of the electron and molecular beams.

B. Size-specific cluster ion dissociation

The properties of molecular clusters are usually found to be intermediate between gas phase and condensed phase behavior, and as such, are important model systems for studying the stepwise evolution to condensed phase properties. Probably the greatest experimental difficulty hindering these studies is the problem of isolating the properties of a single cluster size. The tunable low-mass rejection filter is a convenient approach for unraveling the chemistry of cluster ions.

1. Photoionization of aniline-$(NH_3)_n$

The aniline-$(NH_3)_n$ cation system (henceforth A^+M_n) was recently the subject of a study to understand the role of stepwise solvation of a reactive ion.[13] Here, we demonstrate the LMF as a means of removing successively larger solvent shells M_n, thereby enabling the isolation of chemical properties from each cluster size. REMPI ionization of the clusters was achieved by exciting at wavelengths longer than the aniline monomer $S_1(0, 0)$ transition at 293.77 nm. The series of mass spectra in Fig. 6 compare the unfiltered spectrum from spectra employing successively greater levels of low-mass filtering. A ten-fold attenuation of intensity of ion mass m with respect to m_0 occurs for $m/m_0 \sim 0.80$–0.85. Clearly, the flat baseline in the low-mass region provides a sensitive background for detecting photoproducts. This capability will be demonstrated shortly for the photodissociation of $(CH_3I)_n^+$ formed by EI ionization.

The LMF method may also be applied to the study of size-specific cluster ion metastable decay. Dissociation products that form after the P1 pulse would appear in the LMF mass spectrum. To increase the time available for observing metastable decay, a field-free reaction period can be introduced by delaying the P2 pulse with respect to the P1 pulse (i.e., τ_{del} in Fig. 2). Recently, we applied this LMF mode of operation to the well-known aniline monomer cation decomposition $C_6H_5NH_2^+ \rightarrow C_5H_6^+$ and determined that the rate of dissociation is reduced by more than an order of magnitude by the addition of just a couple of NH_3 solvent molecules to the parent ion.[21]

2. EI ionization of $(NH_3)_n$ and $(NO_2)_n$

EI ionization in a molecular beam is a useful method for assessing neutral cluster distributions and for studying the properties of ion-molecule properties in clusters.[22,23] By using low-energy electrons, it is possible to achieve near threshold ionization conditions and ion cluster distributions that have suffered little fragmentation. The LMF method is suitable for use with EI ionization, however, the cutoff mass resolution for unfocussed electron-beam excitation will generally be less than for focussed laser photoionization. An example of low-mass filtering of a rather diffuse ionization volume is presented in Fig. 7 for EI ionization of $(NH_3)_n$

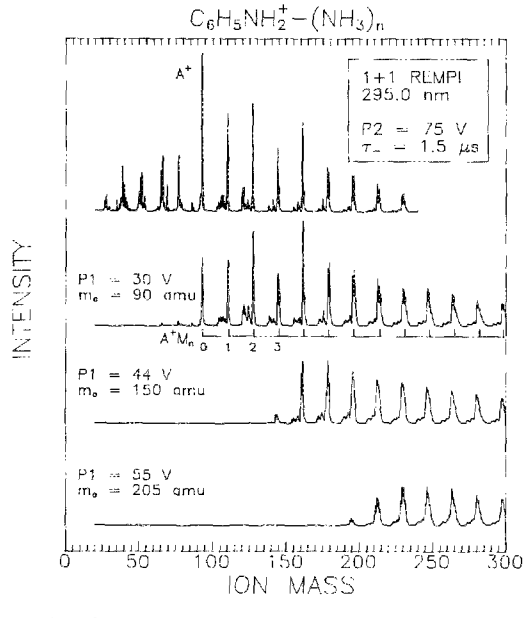

FIG. 6. A series of mass spectra showing successively higher levels of low-mass filtering of aniline cation (A^+) solvated by an ammonia cluster shell (M_n). The top trace is unfiltered (i.e., P1 = 0). Ionization conditions were 1 + 1 REMPI using pulses of 295 nm, 5 ns, and 1.0 mJ. The deflector voltages were adjusted to enhance the detection of larger clusters.

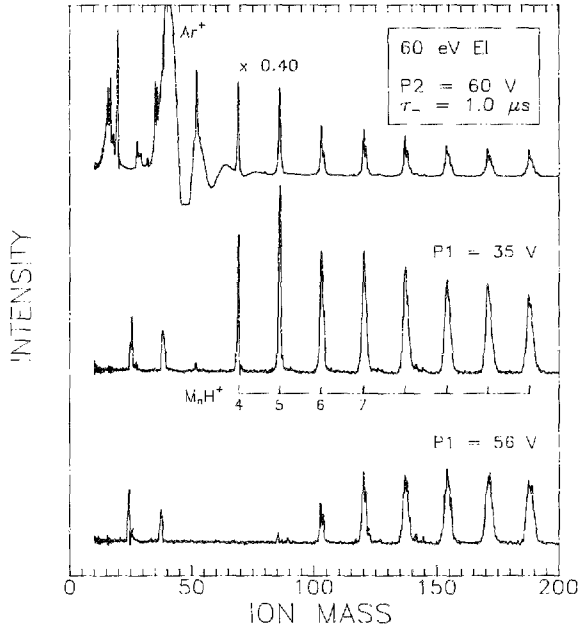

FIG. 7. Series of EI mass spectra of $(NH_3)_n^+$ clusters for various LMF cutoff conditions. Conditions were 60-eV EI ionization and 17% NH_3 in 25-psi Ar. The deflector voltages were adjusted to enhance the detection of larger clusters.

clusters. The low-mass rolloff is not as steep as for REMPI ionization (Fig. 6). Nonetheless, a ten-fold rejection ratio is observed for ion masses $m/m_0 \sim 0.75$–0.80, enabling near complete isolation of adjacent cluster sizes up to $n = 5$. Similar results were obtained when using a sample of $(NO_2)_n$ clusters. The Ar^+ signal at 40 amu in Figs. 7(b) and 7(c) has an intensity of less than 1% of the unfiltered signal in Fig. 7(a), and is believed to occur by ionization of background Ar in the region between grids V1 and V0. The spurious signal appearing at 23 amu is most likely due to another mass whose TOF arrival time was disrupted by perhaps delayed metastable formation or collision induced ionization.

3. Photodissociation of $(CH_3I)_n^+$ cluster ions

A means for studying photodissociation from specific ion cluster sizes is illustrated in Fig. 8 for $(CH_3I)_2^+$. Mass spectra are presented that represent the sequence of events: ionization, low-mass rejection, and photodissociation. The 30-eV EI ionization mass spectrum is shown in Fig. 8(a). The LMF P1 pulse was then adjusted to remove all masses below the dimer ion [$m_0 = 200$ amu, Fig. 8(b)]. A spectrum consisting of *only* the dimer species is obtained by subtracting, from Fig. 8(b), the mass spectrum in which the LMF P1 pulse removes all masses below the trimer ($m_0 = 350$ amu). This difference spectrum is presented in Fig. 8(c) for the case where no photodissociation was involved. By this method, a window of ion masses $200 < m < 350$ amu is selected. The mass window can be made narrower for more demanding mass discrimination needs. The corresponding difference spectrum for the presence of a 595-nm resonance dissocation pulse reveals, in Fig. 8(d), the photoproduct for dimer cation dissociation. We are successfully applying LMF photodissociation mass spectroscopy to the study of larger cluster ions.[21,24]

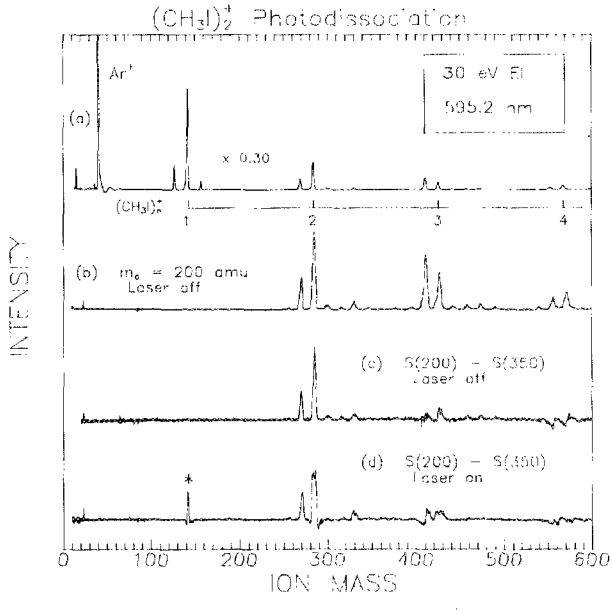

FIG. 8. Mass specific resonance photodissociation of $(CH_3I)_2^+$. (a) 30-eV EI mass spectrum (Ar^+ peak has been clipped and is ~3× larger than shown). (b) LMF rejection of monomer CH_3I^+ (P1 = 50 V, τ = 1.2 μs). (c) Window spectrum for dimer only, obtained from the difference of the LMF spectra $S(m_0)$ for m_0 = 200 and m_0 = 350 amu. (d) Corresponding difference spectrum showing dimer photodissociation to CH_3I^+ (*) (595.2 nm, 35 mJ, unfocused). The deflector voltages for all spectra were adjusted to enhance the detection of larger clusters.

The sensitivity of detecting cluster ion photodissociation is mostly determined by the effectiveness of the LMF and the extent to which collision induced dissociation (CID) interferes with the photofragment signal. CID frequently occurs in mass-selective dissociation experiments that depend on tandem mass analyzers because of the large distance between the mass separation site and the photodissociation site. This is preferable when CID is the main focus of study,[25] however, it can hinder the study of photodissociation. In the LMF method, the mass-selected ions travel about 1 cm between ionization and photodissociation. As a result, CID is negligible as witnessed by the absence of fragment ions for laser off conditions [e.g., Fig. 8(b)]. We can only gain a rough estimate of the sensitivity of detecting cluster ion photodissociation because it is difficult to know the cluster ion densities. The density of ion clusters for $n \geqslant 3$ are about an order of magnitude less than for the monomer ion ($\sim 5 \times 10^5$ cm^{-3}). Assuming, then, a trimer ion density of 5×10^4 cm^{-3}, and an observed signal-to-noise ratio for detection of the dimer cluster ion fragment of about 30 (with 100-pulse averaging), one arrives at a photodissociation detection limit on the order of 10^3 cm^{-3}. As mentioned earlier (Sec. III A), the sensitive detection limit benefits from the large ionization volume defined by the EI beam diameter.

IV. DISCUSSION

One of the many problems facing ion photodissociation studies is distinguishing the photoproducts from the initially formed ionization fragments of the same mass. This difficulty becomes more acute in cluster ion studies where the parentage of the photoproducts is not easily assigned. We have demonstrated a technique, based on a single TOF mass analyzer, that enables mass selective excitation *and* detection of photodissociation and metastable decay in ions and cluster ions. The technique is extremely sensitive to the detection of ion photofragments ($\sim 10^3$ parent ions/cm^3). Alternative methods that offer these capabilities depend on double mass spectrometer designs that are specific to the study of ion dissociation and ion chemistry. Although these methods offer high levels of mass discrimination, the ionization and photodissociation regions are usually well separated and, hence, the ion packet tends to spread in volume, causing decreased ion densities. In the present technique, the separation of the ionization and dissociation volumes is minimized. Consequently, the ion packet for a specific mass is tightly bunched; a situation that favors experiments that require high sensitivity and/or multiphoton dissociation. The short excursion also discriminates against the interfering process of collision-induced dissociation.

The present technique does not compete with tandem mass spectrometer designs in the ultimate limits of ion mass selectivity. However, the LMF method offers a favorable combination of sensitivity and mass selectivity that should prove suitable to a large class of photodissociation studies.

Most importantly, the study of mass specific photodissociation of cold ion and cluster ion species is now within the reach of a much larger realm of molecular-beam mass spectrometer instruments.

ACKNOWLEDGMENTS

I am grateful for the software assistance provided by Eric Fournier. Discussions with James Pollard were also of great benefit. This work was supported by the Aerospace Sponsored Research program.

APPENDIX

The threshold conditions separating ion trajectories that penetrate the lower grid (absorbing boundary condtion) versus those that are reflected, are found by solving for trajectories whose minima occur precisely at $s = 0$ (i.e., the position of the lower grid). This is achieved by evaluating Eqs. (1) or (2) for the condition

$$v(t + t_i) = 0, \qquad s(t + t_i) = 0. \tag{A1}$$

We define two time intervals: $\tau_1 = t_1 - t_0$ denotes the fixed duration of the LMF rejection field E_1, and $t = t_2 - t_1$ represents the subsequent extraction period under field strength E_2. Solving for Eq. (A1), one obtains from Eqs. (1) and (2),

$$s(t + \tau_1) = 0 = s(t_0) + v(t_0)(t + \tau_1) + \frac{0.965 E_1 \tau_1 t}{m} + \frac{0.482}{m}(E_1 \tau_1^2 + E_2 t^2), \tag{A2}$$

$$v(t + \tau_1) = 0 = v(t_0) + \frac{0.965}{m}(E_1 \tau_1 + E_2 t), \tag{A3}$$

where $q = +1$ for positive ions. For the initial conditions $t_0 = 0$, $v(0) = 0$ and $s(0) \equiv s_0 > 0$, $v(t + \tau_1)$ can only equal zero if E_1 and E_2 are of opposite sign. The more specific conditions stated by Eq. (A1) require $E_1 < 0$ and $E_2 > 0$. Equating the right hand sides of Eqs. (A2) and (A3) and rearranging, leads to the expression

$$m s_0 = 0.482 \frac{E_1 (E_1 - E_2)}{E_2} \tau_1^2. \tag{A4}$$

Equation (A4) is equivalent to Eq. (3) if we relate $E_1 = E$ and $E_2 = E_+$ and express s as a fractional distance x between the lower ($x = 0$) and upper ($x = 1$) grids.

The transmission function $T(m)$ for detection of ion mass m is obtained by integrating over the ion density distribution $n(x)$. For a particular m, there is a distinct threshold position x_m that separates ions that are rejected ($x < x_m$) from ions that are detected ($x > x_m$). The fraction of ions that are detected is given by

$$T(m) = \int_{x_m}^{1} n(x)dx \Big/ \int_{0}^{1} n(x)dx \tag{A5}$$

We adopt the $n(\theta) = \cos^2 \theta$ distribution assumed for free jet expansion.[17] Converting to radial coordinates (by the transformation $x - x_0 = z \tan \theta$, where z is a constant, and $x_0 \equiv x(0)$ is the center position of the ion distribution), the distribution function $n(x)$ becomes

$$n(x) = \frac{1}{1 + [(x - x_0)/\Delta x]^2} \tag{A6}$$

where Δx is the full width at half maximum (FWHM) of the ion density distribution expressed as a fraction of the grid spacing. The integrals in Eq. (A5) are easily solved to give the expressions in Eq. (4). A more rigorous treatment would evaluate the integrations in Eq. (A5) over $[n(x)]^2$ to account for the ion distribution orthogonal to the x direction and the molecular beam direction. The integration is solvable, but the resulting expressions are more cumbersome. Such a treatment causes the transmission curves in Fig. 4 to appear moderately sharper for a particular value of Δx.

[1] T. A. Miller and V. E. Bondybey, Eds. *Molecular Ions: Spectroscopy, Structure and Chemistry* (North-Holland, New York, 1983), p. 125.
[2] J. A. Syage and J. E. Wessel, Appl. Spectrosc. Rev. **24**, 1 (1988).
[3] (a) R. G. Keesee and A. W. Castleman, Jr., in *Ion and Cluster Ion Spectroscopy and Structure*, edited by J. P. Maier (Elsevier, New York, 1989) p. 275; (b) T. D. Mark and A. W. Castleman, Jr., Adv. At. Mol. Phys. **20**, 65 (1985).
[4] J. T. Moseley, Adv. Chem. Phys. **40**, 245 (1985).
[5] R. C. Dunbar, in *Ionic Processes in the Gas Phase*, edited by M. A. Almoster Ferreira (Reidel, Boston, 1984), p. 179.
[6] A. G. Marshall, Acc. Chem. Res. **18**, 316 (1985).
[7] R. J. S. Morrison, W. E. Conway, T. Ebata, and R. N. Zare, J. Chem. Phys. **84**, 5527 (1986); P. O. Danis, T. Wyttenbach, and J. P. Maier, J. Chem. Phys. **88**, 3451 (1988).
[8] M. Okumura, L. I. Yeh, and Y. T. Lee, J. Chem. Phys. **83**, 3705 (1985); M. Okumura, L. I. Yeh, J. D. Meyers, and Y. T. Lee, J. Chem. Phys. **85**, 2328 (1986).
[9] L. A. Bloomfield, R. R. Freeman, and W. L. Brown, Phys. Rev. Lett. **54**, 2246 (1985).
[10] Q.-L. Zhang, Y. Liu, R. F. Curl, F. K. Tittle, and R. E. Smalley, J. Chem. Phys. **88**, 1670 (1988); S. M. Beck and J. Andrews, *ibid.* **91**, 4420 (1989).
[11] O. Echt, P. D. Dao, S. Morgan, and A. W. Castleman, Jr., J. Chem. Phys. **82**, 4076 (1985).
[12] U. Boesl, H. J. Neusser, R. Weinkauf, and E. W. Schlag, J. Chem. Phys. **86**, 4857 (1982).
[13] J. A. Syage, J. Phys. Chem. **93**, 170 (1989).
[14] W. C. Wiley and I. H. McLaren, Rev. Sci. Instrum. **26**, 1150 (1955).
[15] J. A. Syage, Chem. Phys. Lett. **143**, 19 (1988).
[16] J. E. Pollard and R. B. Cohen, Rev. Sci. Instrum. **58**, 32 (1987).
[17] J. B. Anderson and J. B. Fenn, Phys. Fluids **8**, 780 (1965); R. E. Smalley, L. Wharton, and D. H. Levy, Acc. Chem. Res. **10**, 139 (1977).
[18] A. M. Woodward, S. D. Colson, W. A. Chupka, and M. G. White, J. Phys. Chem. **90**, 274 (1986); W. A. Chupka, S. D. Colson, M. S. Seaver, and A. M. Woodward, Chem. Phys. Lett. **95**, 171 (1983).
[19] K. Walter, R. Weinkauf, U. Boesl, and E. W. Schlag, J. Chem. Phys. **89**, 1914 (1988); R. Weinkauf, K. Walter, U. Boesl, and E. W. Schlag, Chem. Phys. Lett. **141**, 267 (1987).
[20] J. A. Syage, J. E. Pollard, and J. Steadman, Chem. Phys. Lett. **161**, 103 (1989).
[21] J. A. Syage, J. Chem. Phys. **92**, 1804 (1990).
[22] J. F. Garvey and R. B. Bernstein, Chem. Phys. Lett. **143**, 13 (1988); J. F. Garvey and R. B. Bernstein, J. Am. Chem. Soc. **109**, 1921 (1987); J. F. Garvey and R. B. Bernstein, J. Phys. Chem. **90**, 3577 (1986).
[23] H. Shinohara and N. Nishi, Chem. Phys. Lett. **87**, 561 (1982); H. Shinohara, N. Nishi, and N. Washida, Chem. Phys. Lett. **106**, 3021 (1984).
[24] J. A. Syage and J. Steadman (unpublished).
[25] D. E. Hunton, M. Hofmann, T. G. Lindeman, C. R. Albertoni, and A. W. Castleman, Jr., J. Chem. Phys. **82**, 2884 (1985).